Slade, *Science* **253**, 1508 (1991).
6. B. Hapke, *Icarus* **88**, 407 (1990).
7. S. Nozette *et al.*, *Science* **274**, 1495 (1996);
8. B. A. Campbell and D. B. Campbell, *J. Geophys. Res.* **97**, 16293 (1992), figure 9 and table 6; J. K. Harmon and S. J. Ostro, *Icarus* **62**, 110 (1985).
9. B. A. Campbell, R. E. Arvidson, M. K. Shepard, *J. Geophys. Res.* **98**, 17099 (1993), figure 11.
10. The incidence angle is the angle between the incident radiation and the local vertical (mean surface normal). Near the lunar poles, the incidence angle for Earth-based observations approaches 90°. An imaging radar system forms a map of the surface backscatter from range-Doppler measurements of backscatter. The projection of range-Doppler coordinates onto a surface at high incidence angles is similar to a regular grid in surface coordinates, resulting in a "plan view" of the surface backscatter.
11. G. L. Gutschewski, D. C. Kinsler, E. Whitaker, *Atlas and Gazetteer of the Near Side of the Moon* (NASA, Washington, DC, 1971).
12. E. M. Shoemaker, M. S. Robinson, E. M. Eliason, *Science* **266**, 1851 (1994).
13. The two senses of circular received polarizations contain the OC and SC components of the backscatter signal. The OC component is the circular polarization sense expected from a single reflection with a plane interface, and the SC component is the orthogonal circular polarization. The main contributions to the backscatter signal are from single quasi-specular reflections (caused by mirrorlike reflection from smooth facets possibly many wavelengths in size) and diffuse scattering mechanisms (arising from wavelength-size surface and near-surface structures). These effects contribute to the OC signal and to both received polarizations, respectively. Backscatter from two successive quasi-specular reflections is not expected to contribute appreciably to the SC signal because of the low intrinsic reflectivity of the lunar surface.
14. In a pulsed-radar experiment, a short burst of energy is transmitted and the echo is received during the transmitter off time. The fraction of the time spent transmitting (the duty cycle) varied from 2% to 15% for our lunar observations.
15. T. Hagfors, *Radio Sci.* **5**, 189 (1970).
16. Double-bounce scattering has been identified in radar observations of the crater Carlini (33.7°N, 24.0°W) in Mare Imbrium where forward scatter from the front inner rim is reflected a second time from the radar-facing inner rim (*1*), and in observations of terrace structures in the rim of the crater Copernicus.
17. The multi-look OC and SC image pixel values are random variables with χ^2 distributions and $2N$ degrees of freedom, where N is the number of independent looks. Assuming that the OC and SC random variables are independent and the local surface is homogeneous (so measurements from adjacent pixels used in the averaging are from the same distribution), the CPR follows an F distribution with $2N$ degrees of freedom. For large N (for example, >25), the fractional SD of the F distribution is given by approximately $(2/N)^{1/2}$.
18. Small features with high CPRs were identified as regions of adjacent pixels (in the up-down and left-right directions, not at 45°) with CPRs > 1.2 from the four-look data. If such a region was found to contain 10 or more pixels, then it was encompassed by a rectangle and the mean OC and SC backscatter of all the pixels within the rectangle and above a signal-to-noise ratio threshold were calculated (a threshold of 15 dB for the OC polarization was used for the south pole data analysis). The CPR for the region was calculated from the ratio of the rectangle mean SC and OC backscatter values. If the cumulative F distribution for the region polarization ratio had a value greater than 0.9773, then the region was accepted as a candidate high-CPR feature. (The cumulative F distribution was used here to test whether a CPR was significantly different from a value of 1.)
19. Most of the absolute backscatter uncertainty is attributable to systematic errors, which apply equally to both the SC and OC cross-section measurements. Consequently, the uncertainty in the CPR (= SC/OC) is almost entirely attributable to the statistical uncertainties in the SC and OC cross sections.
20. We thank P. Perillat, A. Crespo, A. Hine, and other support staff at the Arecibo Observatory who helped to make these lunar observations possible. Supported in part by NASA grant NAGW 3985 from the Planetary Geology and Geophysics program. The National Astronomy and Ionosphere Center is operated by Cornell University under a cooperative agreement with NSF, and is also supported by NASA.

6 February 1997; accepted 23 April 1997

The Source of Green Light Emission Determined from a Heavy-Ion Storage Ring Experiment

D. Kella, L. Vejby-Christensen, P. J. Johnson, H. B. Pedersen, L. H. Andersen*

The final electronic states of oxygen atoms formed by dissociative recombination of O_2^+ with cold electrons have been measured by an imaging technique at a heavy-ion storage ring. The ^3P, ^1D, and ^1S quantum yield for O_2^+ in the vibrational ground level was found to be 0.86, 1.09, and 0.05, respectively. The yield of the ^1S state, which is responsible for the 5577 angstrom green light from upper planetary atmospheres, was more than an order of magnitude larger than the theoretical value used in atmospheric models. The results may help refine the models of the chemistry and dynamics of the ionosphere and provide guidance for further quantum-chemistry calculations.

During the daytime, the atmosphere is exposed to ultraviolet sunlight that creates ionized molecules like O_2^+. At nighttime, the molecular ions may recombine with electrons and dissociate into atomic fragments with electronic excitation. The subsequent emission of light from excited atoms in the atmosphere gives rise to several characteristic lines in the emission spectrum. The green line at 5577 Å, which is a prominent feature of the spectrum of the night sky, was detected more than 100 years ago by Campbell (*1*). In 1927 McLennan and co-workers suggested that the origin of this line is the forbidden transition in atomic oxygen $^1S \rightarrow {}^1D$ (*2*). A few years later Kaplan (*3*) suggested that the excited O(^{1}S) atoms might be a product of dissociative recombination (DR), and in 1947 Bates and Massey (*4*) pointed out that DR of O_2^+ was indeed the only process that could explain the observed electron recombination rates in the ionosphere of Earth (≥100-km altitude).

Knowledge of the rate of production of O atoms in different electronic states is important for aeronomers who extensively use the 5577 Å O(^{1}S) green line emission as a source of information about the chemistry and dynamics of the ionosphere (*5*, *6*). Despite many years of experimental and theoretical research, the distribution of specific excited states of atomic oxygen as a result of DR is still uncertain. The interpretation of laboratory as well as observational data has been difficult and controversial due to the lack of such knowledge. For example, the expectation of a very low fraction of oxygen atoms in the ^1S excited state has led to speculation that an unknown source of O(^{1}S) might exist in the atmosphere, or the O_2^+ ions might have an unusually high degree of vibrational excitation that causes an enhanced ^1S yield (*7*, *8*). Molecular oxygen ions are abundant in the atmosphere of Earth as well as in the atmospheres of other planets like Mars and Venus. Because DR provides neutral oxygen atoms with a kinetic energy that depends on their final electronic states, the branching ratios for formation of oxygen in the various electronic states are needed to model the heating of such atmospheres as well as for determining the continuous escape of atoms from the atmospheres (*9*, *10*).

The DR of O_2^+ with low-energy electrons ($E \approx 0$) may be written as

$$e^-_{E\approx 0} + O_2^+ \rightarrow O + O + \text{kinetic energy} \quad (1)$$

It involves transformation of potential and kinetic energy from the incoming electron, e^-, into electronic excitation and kinetic energy of the atoms after dissociation of the molecule. To understand the direct DR process, in which the electron is captured into a doubly excited repulsive electronic state, knowledge about the initial potential-energy curve of the molecular ion, the repulsive curves of the excited, neutral molecule, and the capture probability of the relevant curves is required. In addition, the progression along the repulsive curves, often with

Institute of Physics and Astronomy, University of Aarhus, DK 8000, Aarhus C, Denmark.

*To whom correspondence should be addressed. E-mail: lha@dfi.aau.dk

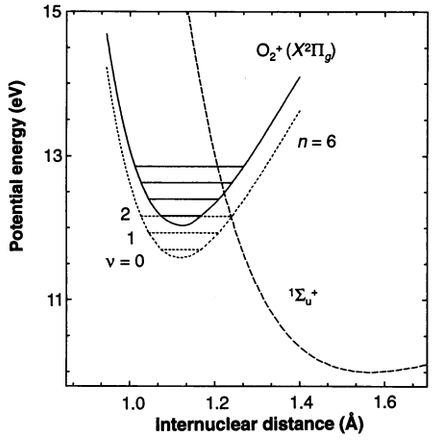

Fig. 1. Potential-energy curves of $O_2^+(X\,^2\Pi_g)$ (solid line) and O_2 (dashed line). The $^1\Sigma_u^+$ repulsive curve of O_2 is believed to be responsible for the production of $O(^1S)$ through the $^1D + {}^1S$ channel. As an example, the lowest vibrational levels of the $n = 6$ Rydberg state (*13*) are shown.

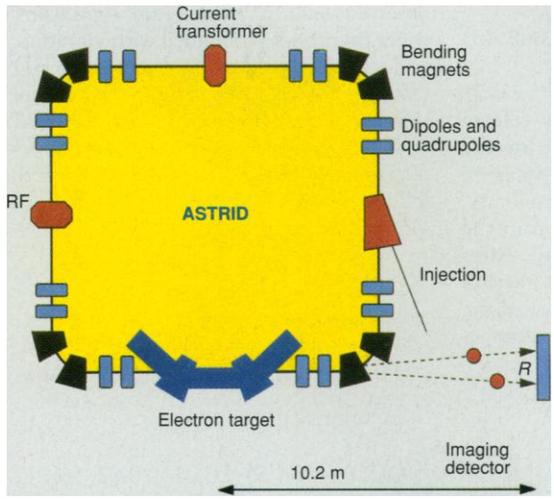

Fig. 2. Schematic diagram of the ASTRID heavy-ion storage ring with the electron target (electron cooler) and imaging detector.

many level crossings to the final atomic limits, must be understood. It also turns out that indirect couplings where electronic energy is transferred into the nuclear motion can be important, and the treatment of such non–Born-Oppenheimer couplings is often needed in DR calculations.

There are a number of channels that are energetically allowed when O_2^+ recombines with electrons. For electrons of zero kinetic energy in the frame of the molecular ion, O atoms may be produced in the following five channels:

$$
\begin{aligned}
&e^- + O_2^+(X^2\Pi_g)(v,J)\\
&\rightarrow O(^3P) + O(^3P) + 6.95\ \text{eV} + E_{v,J}\ (N_a)\\
&\rightarrow O(^3P) + O(^1D) + 4.99\ \text{eV} + E_{v,J}\ (N_b)\\
&\rightarrow O(^1D) + O(^1D) + 3.02\ \text{eV} + E_{v,J}\ (N_c)\\
&\rightarrow O(^3P) + O(^1S) + 2.77\ \text{eV} + E_{v,J}\ (N_d)\\
&\rightarrow O(^1D) + O(^1S) + 0.80\ \text{eV} + E_{v,J}\ (N_e)
\end{aligned}
\qquad (2)
$$

where v is the vibrational quantum number, J is the rotational quantum number, $E_{v,J}$ is the contribution of the initial rovibrational level to the kinetic energy release, and N_f ($f = a, b, \ldots e$) denotes the branching ratios.

Guberman identified the $^1\Sigma_u^+$ repulsive valence potential-energy curve associated with the $O(^1D) + O(^1S)$ atomic limit as the only channel through which the direct electronic interaction significantly leads to the production of $O(^1S)$ from the lowest vibrational levels of O_2^+ (*11*, *12*). Because this curve does not cross the O_2^+ ground-state potential-energy curve within the classical turning points of the $v = 0$ level (Fig. 1), it was expected that the $O(^1S)$ yield from DR of O_2^+ in the vibrational ground level is small. The rate coefficient for dissociation to the $O(^1S) + O(^1D)$ limit through the $^1\Sigma_u^+$ repulsive potential energy curve was calculated (*11*) by a comparison with the experimental total rate coefficient, and it was concluded that the quantum yield for $O(^1S)$ from $v = 0$ was as low as 0.0016. It was assumed that no other channels contribute to the $O(^1S)$ production. It was also predicted that the DR rate along the $O_2(^1\Sigma_u^+)$ curve increases when vibrationally excited O_2^+ is considered because the Franck-Condon overlap between the vibrational wave functions of the electronic ground state of O_2^+ and the continuum wave functions of the $^1\Sigma_u^+$ repulsive curve is increased for the higher vibrational levels. In a later calculation, taking into account indirect electronic-nuclear channels, Guberman and Giusti-Suzor (*13*) calculated an even lower rate coefficient resulting in a ^1S quantum yield of 0.0012 for $v = 0$.

Our experiment was carried out at the ASTRID heavy-ion storage ring in Aarhus, Denmark (*14*). ASTRID has a square structure with four straight sections of about 8 m each and two 45° bending magnets in the corners. A total of 16 quadrupole magnets and 16 correction dipoles are used to steer and focus the ion beam. An average pressure of about 3×10^{-11} torr provided a storage lifetime sufficiently long that measurements could be performed over a time period of 30 s. The storage technique ensured that electronically metastable states of O_2^+ such as the $a^4\Pi_u$ state with a lifetime of about 0.1 s (*15*) decay completely before the measurement. During the storage time, partial vibrational relaxation was obtained by the use of the $^{18}O^{16}O^+$ molecular ion, which has an intrinsic dipole moment. The vibrational radiative lifetime of the $v = 1$ level in the $X^2\Pi_g$ electronic ground state is calculated to be 25 s (*16*). Problems associated with collisional quenching of excited oxygen atoms, which may be encountered in plasma experiments, are avoided in the ring experiment because we study single O_2^+ molecular ions that recombine with free electrons in an ultra–high vacuum environment. Efficient detection of the DR products is provided by measuring in coincidence the two atoms by a particle detector (Fig. 2).

The $^{18}O^{16}O^+$ ions were produced by a radiofrequency ion source from a gas mixture containing ^{18}O and ^{16}O. The ions were first accelerated to 150 keV and then injected into the storage ring. After injection the beam was accelerated to 4.5 MeV. Nine seconds after injection the ions were merged with electrons at equal speed (corresponding to an energy of ~72 eV), and data were collected from 10 to 30 s after the injection. The electrons were produced by the electron cooler at ASTRID (*17*, *18*) that provides a magnetically confined, adiabatically expanded electron beam with an energy spread characterized by a Boltzmann distribution with a transverse temperature of about 20 meV ($T \sim 200$ K) and a longitudinal temperature of about 0.1 to 1 meV ($T \sim 1$ to 10 K). Neutral fragments from the DR process passed through the bending magnet after the electron target and were detected by an imaging detector located about 5 m behind the magnet. The detector was a 77-mm-diameter microchannel-plate detector with a phosphor anode. The light from the anode was recorded by a charge-coupled-device camera, and the projected distance between pairs of atoms was measured.

To analyze the imaging data, we used the following formulation: Let E_i be the kinetic energy of the molecular ion at the time of recombination, θ the angle between the internuclear axis and the beam direction, and L the distance from the place of recombination to the imaging detector. Then the distance, R, measured on the detector is

$$R = \sqrt{\frac{\Delta E_k}{E_i}}\frac{M_1 + M_2}{\sqrt{M_1 M_2}} L\sin\theta = R_{max}\sin\theta \quad (3)$$

where ΔE_k is the kinetic energy release and M_1 and M_2 are the masses of the atomic fragments. Because the imaging data were taken at zero relative velocity, we assume an isotropic distribution in the rest frame of the molecular ion. After integration over the finite interaction length ΔL (1 m), we obtain the following expression for the distribution of distances between fragments:

$$F(R) = \frac{1}{c\Delta L} \times \left[\arctan\frac{K(L_2)}{R} - \arctan\frac{K(L_1)}{R}\right] \quad (4)$$

where $L_1 = L_0 - \Delta L/2$, $L_2 = L_0 + \Delta L/2$, and $K(L_i) = Re\sqrt{(cL_i)^2 - R^2}$, L_0 being the distance from the center of the interaction region to the imaging detector (10.2 m) and $c = R_{max}/L$. Equation 4 predicts the shape of the distribution of projected distances for a single value of the kinetic-energy release. It describes satisfactorily the case with only one vibrational level of the ion and one final electronic limit that is found for rotational cold HD^+ (*19*, *20*). Here we deal with rotationally excited ions by assuming that the cross section has negligible rotational dependence and that the rotational population is given by a Boltzmann distribution, with a single temperature T, independent of the vibrational excitation. If the population of the vibrationally excited levels is given by $p(v)$, the final distribution of projected distances becomes

$$D(R) = \sum_J (2J + 1)e^{\frac{-J(J+1)B}{kT}} \times \sum_v \sum_{f=a-e} P(v,f)F(R) \quad (5)$$

where B is the rotational constant, k is Boltzmann's constant, v is the vibrational quantum number, f is the final electronic channel of the dissociation products, and $P(v,f) = \text{constant} \cdot p(v) \cdot \langle v\sigma_{v,f}(v)\rangle$, where $\langle v\sigma\rangle$ is the DR rate coefficient at zero relative energy, which is averaged over the electron-velocity distribution. $F(R)$ depends on the vibrational and rotational state through the kinetic-energy release. The function $D(R)$ was used to fit the experimentally obtained imaging data with kT and $P(v,f)$ as fitting parameters. For a given $v = v_0$ the branching ratios N_f ($f = a, b, \ldots e$) are directly proportional to $P(v_0,f)$.

The O_2 imaging data (yield as a function of projected distance R) exhibit peaks that are related to the final electronic channels of the oxygen atoms. To account for the observed features, which are significantly wider than what is obtained with vibrational and rotational cold molecular ions like HD^+ (*19*, *20*), the data were fitted with the function $D(R)$, including six vibrational levels (v = 0 to 5) and rotational levels up to J = 60.5 (Fig. 3). The result of the fit yields the following branching ratios for O_2^+ in the vibrational ground state (v = 0):

$$O(^3P) + O(^3P) : 0.22 + 0.10 \quad (N_a)$$

$$O(^3P) + O(^1D) : 0.42 \pm 0.05 \quad (N_b)$$

$$O(^1D) + O(^1D) : 0.31 \pm 0.07 \quad (N_c)$$

$$O(^3P) + O(^1S) : <0.01 \quad (N_d)$$

$$O(^1D) + O(^1S) : 0.05 \pm 0.02 \quad (N_e) \quad (6)$$

and thus the ^3P, ^1D, and ^1S quantum yields (*21*) are 0.86 ± 0.15, 1.09 ± 0.15, and 0.05 ± 0.02, respectively. The uncertainties represent absolute lower and upper limits and include statistical, fitting, and calibration uncertainties (including a variation of the rotational temperature from 0 to 0.3 eV). The v = 0 and v = 1 peaks of the $^1D + {}^1S$ channel are separated by more than 1 mm, which is more than the spatial resolution in this region of distances (*19*).

The $O(^3P) + O(^1S)$ channel is theoretically predicted to be zero (*12*), which is consistent with our data. The $O(^3P) + O(^1S)$ channel was also found to be small compared to the $O(^1D) + O(^1S)$ channel from an analysis of data from the Atmosphere Explorer (*22*). The $O(^1D) + O(^1S)$ channel is responsible for the $O(^1S)$ quantum yield and is more than an order of magnitude larger than the theoretical prediction of 0.0012 to 0.0016. The ^1D quantum yield is in good agreement with the generally accepted value of about 1 (*7*).

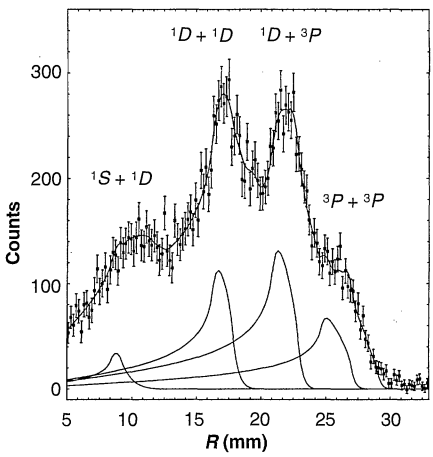

Fig. 3. The distribution of projected distances for $^{18}O^{16}O^+$. Shown are the data with error bars and the fit to the data. The contribution from v = 0 is shown specifically for each final electronic channel.

Summed over all six vibrational levels in the O_2^+ beam, our ^3P, ^1D, and ^1S quantum yields are 0.89 ± 0.04, 1.02 ± 0.04, and 0.09 ± 0.02, respectively. The ^1S quantum yield of the broad vibrational distribution is about a factor of 2 larger than that of the vibrational ground state. In comparison, the ^3P and ^1D quantum yields do not show a significant dependence on the vibrational population of O_2^+. Unfortunately, the exact vibrational population in our experiment, $p(v)$, cannot be deduced from the data without knowledge about the DR cross sections.

It is interesting to compare our results with previous related experimental studies. Helm and collaborators studied dissociation of O_2 in Rydberg states (*23*) and found the $O(^3P) + O(^1S)$ channel to be negligible. Moreover, the branching ratio of the $O(^1D) + O(^1S)$ channel was 0.03, which is in good agreement with the present work. An earlier experimental study of the O_2^+ DR-quantum yield was reported by Zipf (*24*), who found an $O(^1S)$ quantum yield of 0.1 [and 0.9 for $O(^1D)$], but it was later debated whether the O_2^+ ions were vibrationally relaxed during the measurement (*25*). In another work by Queffelec *et al.* (*26*), numerical simulations of the neutral oxygen density in a plasma-flow tube indicated that the ^1S quantum yield for v = 0 and v = 1 (assumed to be equal) was 0.1. However, as in the work by Zipf, the v = 0 contribution was not isolated. Both of these results (*24*, *26*) are consistent with our result for the total yields summed over all vibrational levels.

As for the comparison with theory, it is worth noting that a Rydberg orbital with $n \sim 4$ to 6 has a classical period that approximately equals the vibrational period of $O_2^+(X^2\Pi_g)$, and the Born-Oppenheimer approximation, which treats the electronic and nuclear motion separately, fails. Such vibrationally excited Rydberg states may hence be formed from a non–Born-Oppenheimer coupling of the electronic and nuclear motions. Because vibrationally excited Rydberg states have an overlap with the repulsive valence $^1\Sigma_u^+$ state leading to $O(^1S) + O(^1D)$ (Fig. 1), one might expect an enhanced $O(^1S)$ yield from predissociation of such states. In the case of zero rotations and without the spin-orbit coupling included this turns out not to be the case, however, because according to theory the interference is generally destructive rather than constructive at low electron energy (*13*). It seems appropriate to investigate if higher order terms in the Hamiltonian, like the spin-orbit or spin-spin interactions that are

normally neglected, can cause the more than 10 times increase in the $O(^1S)$ yield derived in our experiment (*27*). Only a relatively small coupling to other dominating DR channels may cause a significant increase in the DR channel leading to $O(^1S)$ (*27*). Furthermore, it seems appropriate to investigate the effect of rotational excitation which, through the energy term $J(J+1)\hbar^2/2\mu R^2$ (where μ is the reduced mass and R is the internuclear distance) perturbs the potential energy curves in a way that may cause an enhanced Franck-Condon overlap of the initial state $O_2^+(X^2\Pi_g, v = 0, J)$ with the repulsive valence $^1\Sigma_u^+$ state.

By our measurement we have demonstrated that the $O(^1S)$ yield from the DR of O_2^+ in the vibrational ground state is not negligible and that DR may be responsible for the 5577 Å green light from upper planetary atmospheres, as suggested many years ago. The information is important for the large number of ground- and satellite-based projects that take advantage of airglow emission lines for determining information about winds, temperatures, heating, density profiles, and escape of atoms from planetary atmospheres. It appears that we have moved a step forward toward a better understanding of the upper atmosphere by addressing this long-standing classical problem in aeronomy. However, we also find a need for better quantum-chemical calculations that address the issue of DR with an improved Hamiltonian and the effect of vibrational and rotational excitation.

REFERENCES AND NOTES

1. W. W. Campbell, *Astrophys. J.* **2**, 162 (1895).
2. J. C. McLennan *et al.*, *Philos. Mag.* **6**, 558 (1928).
3. J. Kaplan, *Phys. Rev.* **38**, 1048 (1931).
4. D. R. Bates and H. S. W. Massey, *Proc. R. Soc. London Ser. A* **192**, 1 (1947).
5. H. Takakashi *et al.*, *Planet. Space Sci.* **38**, 547 (1990).
6. G. G. Shepherd *et al.*, *J. Geophys. Res.* **98**, 10725 (1993).
7. D. R. Bates, *Planet. Space Sci.* **38**, 889 (1990).
8. E. C. Zipf, *ibid.* **36**, 621 (1988).
9. J. L. Fox, *ibid.*, p. 37.
10. ———, *Geophys. Res. Lett.* **20**, 1847 (1993).
11. S. L. Guberman, *Nature* **327**, 408 (1987).
12. ———, *Int. J. Quantum Chem.* **S13**, 531 (1979).
13. ——— and A. Giusti-Suzor, *J. Chem. Phys.* **95**, 2602 (1991).
14. S. P. Møller, in *Conference Record of the 1991 IEEE Particle Accelerator Conference*, San Francisco, CA, 6 to 9 May 1991, L. Lizama and J. Chew, Eds. (IEEE, New York, 1991), p. 2811.
15. C. H. Kuo *et al.*, *J. Chem. Phys.* **92**, 4849 (1990).
16. Z. Amitay *et al.*, *Phys. Rev. A* **50**, 2304 (1994).
17. L. H. Andersen *et al.*, *ibid.* **41**, 1293 (1990).
18. L. Vejby-Christensen *et al.*, *ibid.* **53**, 2371 (1996).
19. L. H. Andersen, P. J. Johnson, D. Kella, H. B. Pedersen, L. Vejby-Christensen, *ibid.* **55**, 2799 (1997).
20. D. Zajfman *et al.*, *Phys. Rev. Lett.* **75**, 814 (1995).
21. The quantum yields are obtained from the branching ratios as follows: $Y[O(^3P)] = 2N_a + N_b + N_d$, $Y[O(^1D)] = N_b + 2N_c + N_e$, and $Y[O(^1S)] = N_d + N_e$.
22. P. B. Hays, V. J. Abreu, S. C. Solomon, J.-H. Yee, *Planet. Space Sci.* **36**, 21 (1988); T. J. Killeen and P. B. Hays, *J. Geophys. Res.* **88**, 10163 (1983).
23. H. Helm, I. Hazell, C. W. Walter, P. C. Cosby, in *Dissociative Recombination: Theory, Experiment and Application*, D. Zajfman, J. B. A. Mitchell, D. Schwalm, B. R. Rowe, Eds. (World Scientific, Singapore, 1996), p. 139.
24. E. C. Zipf, *Bull. Am. Phys. Soc.* **15**, 418 (1970).
25. ———, *J. Geophys. Res.* **85**, 4232 (1980).
26. J. L. Queffelec, B. R. Rowe, F. Vallee, J. C. Gomet, M. Morlais, *J. Chem. Phys.* **91**, 5335 (1989).
27. S. L. Guberman, paper presented at the American Physical Society Meeting, Washington, DC, 18 to 21 April 1977.

28. Supported by the Danish National Research Foundation through the Aarhus Center for Advanced Physics and the Human Capital and Mobility Programme of the European Community. L.H.A. is indebted to JILA, University of Colorado, for hospitality during his 1996–1997 Visiting Fellowship. We thank the staff at the ASTRID storage ring for help and support during the measurements and W. C. Lineberger and D. Nesbitt for comments on the manuscript.

25 February 1997; accepted 29 April 1997

Design of Surfaces for Patterned Alignment of Liquid Crystals on Planar and Curved Substrates

Vinay K. Gupta and Nicholas L. Abbott*

Molecularly designed surfaces formed by chemisorption of alkanethiols on ultrathin films of gold permit control of both the azimuthal and polar orientations of supported nematic liquid crystals (LCs). These surfaces, when patterned, form simple and versatile templates for the fabrication of complex optical structures from LCs. Surfaces patterned with odd or even alkanethiols, or mixtures of long and short alkanethiols, were used to fabricate tunable, micrometer-scale LC diffraction gratings that differed in their polarization sensitivity. Patterned alignment of LCs on curved surfaces is also demonstrated, thereby providing principles for fabrication of optical elements that combine diffractive and refractive optics.

Past interest in the orientations assumed by LCs near surfaces has been largely driven by their use in electrooptical devices such as flat-panel displays (FPDs). A goal of many studies has, therefore, been the development of methods for the fabrication of surfaces that uniformly orient LCs over large areas. Future uses of LCs in electrooptic devices, in contrast, will rely increasingly on LCs with patterned orientations over small areas (*1*–*5*). For example, light can be diffracted or redirected by using patterned LC structures that are tuned by application of a uniform electric field (*5*), and FPDs with wide viewing angles and broad gray scales can be fabricated by using pixels that are divided into subpixels, where each subpixel is defined by a different orientation of the LC (*6*). Methods capable of patterning LCs on curved surfaces are also required for the development of new types of tunable electrooptic LC devices, including devices that combine the diffraction of light from the patterned LC structure with the refraction of light at the curved surface (*7*).

Current procedures for the fabrication of patterned LC structures use either spatially nonuniform electric fields from patterned electrodes or patterned "anchoring" surfaces. Fringing of electric fields from patterned electrodes prevents high-resolution patterning of LCs by this method (*1*, *8*). Patterned anchoring surfaces have been prepared by using mechanical rubbing of spin-coated polymer films, photolithographic masking, and a second rubbing step performed in a direction orthogonal to the first (*3*, *5*, *9*). This method of patterning LCs on surfaces is complex and suffers from the disadvantages of rubbing-based methods, such as the generation of dust and static charge. Recently developed photo-alignment techniques for orienting LCs provide promising alternatives (*1*, *6*, *10*). However, because light-based methods generally require surfaces to be spin-coated by uniformly thin films of photopolymer, and because the orientations of LCs on photo-aligned surfaces are determined by the angle of incidence of the light used for alignment, these methods are not easily applied to the patterning of LCs on nonplanar surfaces.

Our approach to the patterning of LCs on flat and curved surfaces is based on the use of patterned self-assembled monolayers (SAMs) of molecules to direct both the polar (away from the surface) and azimuthal (in the plane of the surface) orientations of LCs supported on surfaces. The methods are simple and flexible, and any of the recently established procedures for patterning SAMs

Department of Chemical Engineering and Materials Science, University of California, Davis, CA 95616, USA.

*To whom correspondence should be addressed. E-mail: nlabbott@ucdavis.edu